

Comparison of a Reference Region Model With Direct Measurement of an AIF in the Analysis of DCE-MRI Data

Thomas E. Yankeelov,^{1–4*} Greg O. Cron,⁵ Christina L. Addison,⁶ Julia C. Wallace,⁸ Ruth C. Wilkins,⁹ Bruce A. Pappas,⁷ Giles E. Santyr,^{8,10} and John C. Gore^{1–4}

Models have been developed for analyzing dynamic contrast-enhanced (DCE)-MRI data that do not require measurements of the arterial input function (AIF). In this study, experimental results obtained from a reference region (RR) analysis are compared with results of an AIF analysis in the same set of five animals (four imaged twice, yielding nine data sets), returning estimates of the volume transfer constant (K^{trans}) and the extravascular extracellular volume fraction (v_e). Student's *t*-test values for comparisons of K^{trans} and v_e between the two models were 0.14 ($P = 0.88$) and 0.85 ($P > 0.4$), respectively (where the high *P*-values indicate no significant difference between values derived from the two models). Linear regression analysis indicated there was a correlation between K^{trans} extracted by the two methods: $r^2 = 0.80$, $P = 0.001$ (where the low *P*-value indicates a significant linear correlation). For v_e there was no such correlation ($r^2 = 0.02$). The mean (absolute) percent difference between the models was 22.0% for K^{trans} and 28.1% for v_e . However, the RR parameter values were much less precise than the AIF method. The mean SDs for K^{trans} and v_e for the RR analysis were 0.024 min^{-1} and 0.06, respectively, vs. 0.002 min^{-1} and 0.03 for AIF analysis. Magn Reson Med 57:353–361, 2007. © 2007 Wiley-Liss, Inc.

Key words: DCE-MRI; tumor pharmacokinetics; reference region; arterial input function; contrast agent

Dynamic contrast-enhanced magnetic resonance imaging (DCE-MRI) involves the serial acquisition of images before and after the injection of a paramagnetic contrast agent

(CA) (1). As the agent enters the tissue region under investigation, it changes the T_1 and T_2 relaxation times of the tissue water and thereby alters the MR signal intensity. As the agent is transported out of the tissue, T_1 and T_2 (and thus the MR signal intensity) return to their baseline values. Therefore, an MR signal intensity time course can be constructed for each image voxel or a selected region of interest (ROI). The theory typically used to analyze these time courses is based on indicator dilution theory (2) and returns estimates of the volume transfer constant (K^{trans}) and the extravascular extracellular volume fraction (v_e). These two parameters have been shown to be sensitive to tumor growth and treatment response (e.g., Refs. 3–5). Most models employed in the quantitative analysis of DCE-MRI data require knowledge of the time course of the concentration of the CA in arterial blood, otherwise known as the arterial input function (AIF). Since the temporal variation of the AIF is very rapid, it is challenging to measure this time course accurately. High-temporal-resolution imaging is required, which is usually achieved at the expense of the signal-to-noise ratio (SNR) and/or spatial resolution. As these models are frequently used to assess tumor vascular heterogeneity, the loss of spatial resolution (by trading it for temporal resolution) is a significant limitation.

As an alternate approach, there has been recent interest in developing models for analyzing DCE-MRI data that do not require direct measurement of the AIF. Such methods are usually referred to as reference region (RR) models (6,7,8,9), and first appeared in the positron emission tomography (PET) literature (10). These models also are derived from indicator dilution theory and involve comparing the signal change in a well characterized “reference tissue” (e.g., muscle) to that in a tissue of interest (TOI) that is less characterized (e.g., a tumor). Since the RR model is based on the same theory as a direct AIF-driven analysis, the two models should, in principle, yield the same estimates. However, to the best of our knowledge, experimental results obtained from an RR analysis have not been directly compared with analysis employing direct AIF measurements in the same animal. The results of such a comparison are presented here.

THEORY

The details of the two models under consideration have been explained extensively elsewhere (2,9). Briefly, assuming fast exchange, the Kety theory describes the flow of CA from the plasma to the extravascular space:

¹Institute of Imaging Science, Vanderbilt University, Nashville, Tennessee, USA.

²Department of Radiology and Radiological Sciences, Vanderbilt University, Nashville, Tennessee, USA.

³Department of Biomedical Engineering, Vanderbilt University, Nashville, Tennessee, USA.

⁴Department of Physics and Astronomy, Vanderbilt University, Nashville, Tennessee, USA.

⁵Biomedical Magnetic Resonance Unit, Catholic University of Louvain, Brussels, Belgium.

⁶Centre for Cancer Therapeutics, Ottawa Health Research Institute, Ottawa, Ontario, Canada.

⁷Institute of Neuroscience, Carleton University, Ottawa, Ontario, Canada.

⁸Department of Physics, Carleton University, Ottawa, Ontario, Canada.

⁹Consumer and Clinical Radiation Protection Bureau, Health Canada, Ottawa, Ontario, Canada.

¹⁰Imaging Research Laboratories, Robarts Research Institute, London, Ontario, Canada.

Grant sponsor: National Institutes of Health; Grant number: NIBIB1K25EB005936–01; Grant sponsors: Canadian Breast Cancer Research Alliance; Ontario Centre for Breast Cancer Imaging Research.

*Correspondence to: Thomas E. Yankeelov, Ph.D., Vanderbilt University Institute of Imaging Science, 1161 21st Avenue South, AA 1105 Medical Center North, Nashville, Tennessee 37232–2310. E-mail: yankeelov@vanderbilt.edu
Received 17 February 2006; revised 4 October 2006; accepted 6 October 2006.

DOI 10.1002/mrm.21131

Published online 00 Month 2007 in Wiley InterScience (www.interscience.wiley.com).

© 2007 Wiley-Liss, Inc.

$$C_{\text{TOI}}(T) = K^{\text{trans}} \int_0^T C_p(t) \exp(-(K^{\text{trans}}/v_e) \cdot (T - t)) dt, \quad [1]$$

where C_{TOI} and C_p are the concentrations of CA in the TOI and blood plasma, respectively, K^{trans} is the CA extravasation rate constant, v_e is the extravascular extracellular volume fraction, and T is a given time after injection of CA (2). The RR model establishes a relationship between C_{TOI} and C_{RR} (CA concentration in the RR) that allows the derivation of a model that is independent of C_p . The result is:

$$C_{\text{TOI}}(T) = R \cdot C_{\text{RR}}(T) + R \cdot [(K^{\text{trans,RR}}/V_{e,\text{RR}}) - (K^{\text{trans,TOI}}/V_{e,\text{TOI}})] \cdot \int_0^T C_{\text{RR}}(t) \cdot (\exp(-K^{\text{trans,TOI}}/V_{e,\text{TOI}} \cdot (T - t))) dt, \quad [2]$$

where $K^{\text{trans,RR}}$ and $K^{\text{trans,TOI}}$ are K^{trans} for the RR and TOI, respectively; $v_{e,\text{RR}}$ and $v_{e,\text{TOI}}$ are v_e for the RR and TOI, respectively; and $R \equiv K^{\text{trans,TOI}}/K^{\text{trans,RR}}$ (9). Equations [1] and [2] were employed in the analysis of the same DCE-MRI data set, which allowed for a direct comparison of the two models. In the previous presentation of the RR model (Eq. [2]), a two-parameter fit was performed because $K^{\text{trans,RR}}$ and $v_{e,\text{RR}}$ were both fixed (9). Here we allow $K^{\text{trans,RR}}$ to vary as well, thereby reducing the number of assumptions on the RR model at the expense of an additional free parameter. All other aspects of implementation are the same as in Ref. 9.

It is noted that neither Eq. [1] or [2] include the effects of a plasma space (typically denoted as v_p). This can lead to significant overestimation of K^{trans} (see Ref. 11 and references cited therein). Also implicit in both Eqs. [1] and [2] is that the effects of delay and dispersion of the injected bolus are assumed to be minimal. Taken together, these assumptions reduce the accuracy of both methods. However, it is not uncommon to exclude v_p in DCE-MRI analysis (1,2).

MATERIALS AND METHODS

Experimental

Approximately 10^6 R3230 adenocarcinoma cells were injected subcutaneously into the hind flank of five male Fischer-344 rats (~350 g; Charles Rivers, Canada). This produced tumors that were allowed to grow to outer diameters of 5–10 mm (3–6 weeks) (12). Just prior to the MRI experiment, flexible plastic catheters were surgically inserted into a jugular vein and a carotid artery to facilitate intravenous bolus injection of CA (0.3 mmol/kg Omniscan; Nycomed, Canada) and arterial blood sampling, respectively. Blood pressure was monitored via the arterial catheter (except during blood sampling) with a BP-1 blood pressure monitor (World Precision Instruments, Sarasota, FL). All procedures were performed under halothane anesthesia. At the end of each experiment, the rats were

killed by barbiturate overdose. All studies were approved by the Carleton University Animal Care Committee.

All experiments were performed at the Carleton Magnetic Resonance Facility with a 1.89T Oxford 30-cm superconducting magnet, an MRRS (Surrey, England) MR 5000 console, and a 12-cm inner diameter transmit/receive birdcage coil tuned to 80 MHz (Morris Instruments Inc., Ottawa, Canada). For DCE-MRI, a gradient-echo pulse sequence was designed to record images with very high temporal resolution for characterization of the AIF in the aorta (0.9 s) and high temporal resolution for tissue (i.e., tumor and muscle; ~5–15 s, depending on the number of slices) (13). One transverse (axial) slice was prescribed on the aorta ~50–100 mm inferior of the heart. We chose the location (along B_0) of this slice by acquiring several different “scout” transverse images (gradient-echo sequence, field of view (FOV) = 80 mm, matrix = 128×128 , TR = 20 ms, TE = 4 ms, flip angle = 90° , slice thickness = 3 mm) and then choosing the location that provided a high aorta signal and good separation (>5 mm) between the aorta and vena cava.

Three to 10 transverse slices were prescribed on the flank at the location of the tumor. The DCE-MRI pulse sequence was programmed so that for each phase-encode line acquired for the flank (regardless of which slice), one phase-encode line was acquired for the aorta. In order to maximize contrast and SNR in both the flank and aorta, the pulse sequence allowed the flank and aorta to have different matrix sizes, TRs, flip angles, and slice thicknesses. The imaging parameters for the flank were as follows: FOV = 80 mm, matrix = 128×64 , TR = 80–260 ms, TE = 4 ms, flip angle = 30° – 60° , number of slices = 3–10, and slice thickness = 2 mm. For the aorta, the parameters were FOV = 80 mm, matrix = 64×32 , TR = 26 ms, TE = 4 ms, flip angle = 30° , one slice, and slice thickness = 5 mm. The total DCE imaging time following CA injection was approximately 6 min.

For each voxel in the flank, we estimated the concentration-vs.-time of CA using the “bookend method” (14). Briefly, the DCE-MRI gradient-echo signal-vs.-time was calibrated to T_1 -vs.-time via two T_1 -measuring saturation recovery pulse sequences performed before and immediately after DCE-MRI. The T_1 -vs.-time for each voxel in tumor or muscle was then converted to CA concentration-vs.-time via the T_1 relaxivity of the CA ($4.3 \text{ mM}^{-1}\text{s}^{-1}$). For each of the two “bookend” T_1 measurements, saturation recovery images were acquired with recovery times ranging from 230 to 5415 ms. For the precontrast T_1 measurement, the recovery times were 230, 318, 418, 534, 670, 837, 1052, 1355, 1872, 3000, 5415 ms, in that order. For the postcontrast T_1 measurement, the recovery times were 230, 321, 429, 560, 728, 963, 1354, 1900, and 2850 ms, in that order. Thus, the total saturation recovery imaging time was ~16 min for the precontrast measurement and ~10 min for the postcontrast measurement. With these images, signal as a function of recovery time was fit to a three-parameter exponential recovery model to extract T_1 . The saturation pulse was adiabatic in order to compensate for any inhomogeneities in the RF transmit field (14). We previously showed that the bookend method provides T_1 -vs.-time data with systematic errors of less than ~10% (14).

The concentration-vs.-time of CA in the aorta was estimated by a combination of arterial blood sampling and phase imaging. The arterial blood sampling was used to sample the AIF at 10 evenly spaced time points covering the fast bolus regime (0–15 s after injection) and at six evenly spaced time points during the washout period (1–6 min after injection). Blood sampling was initiated at the start of the CA injection. Ten blood samples (volume of each sample = $44 \pm 22 \mu\text{L}$) were taken at 1.5-s intervals. Thereafter, a larger blood sample ($86 \pm 37 \mu\text{L}$) was taken every minute until the end of the DCE-MRI scan. The dead volume of the PE tubing in the carotid artery was $70 \mu\text{L}$. We collected blood from the PE tubing by simply allowing the blood to flow freely out of the end of the tubing. We estimated the concentration of CA in each sample of blood by measuring precisely the mass of the blood withdrawn, diluting the blood in a known volume of heparinized water, and then measuring the T_1 of the solution as described previously (15). This measurement provides the CA concentration in the blood sample with an error of $<7\%$.

For gradient-echo MRI, the phase of a voxel in the (complex) image is defined as the angle of the average transverse magnetization vector (at TE) with respect to a fixed axis in the rotating frame (e.g., the fixed axis defined by the B_1 excitation field). As the CA passes through a blood vessel oriented parallel to the main magnetic field, the gadolinium (Gd) induces a change in phase of that blood proportionately to the change in CA concentration. This relationship is highly linear and well quantified, and essentially depends only on the main magnetic field strength, the TE, and the molar susceptibility of the CA (which is the same for most Gd-based CAs used clinically) (15). For the current study, we calculated the phase-vs.-time of the blood inside the aorta from the DCE-MRI data in order to measure the shape of the fast bolus regime (zero to several seconds after injection) of the AIF at high temporal resolution (0.9 s) (15). The arterial blood sampling data and phase-vs.-time data were combined to calculate the AIF. The AIF was set to zero for all times before injection of CA. The fast bolus regime of the AIF was defined as the time of injection (time zero) up to and including the time after the peak of the AIF where the AIF begins to plateau out (slope $> -2 \text{ mM s}^{-1}$). For the fast bolus regime, the AIF was calculated as the change in phase as a function of time (relative to preinjection baseline values) multiplied by the peak blood sampling value, divided by the peak change in phase. The phase data were scaled to the blood sampling data in this way because of concerns over the lack of precision of the current phase technique (largely due to problems with partial-volume effects) (15). From the end of the fast bolus regime up to the end of the DCE-MRI experiment, the AIF was calculated directly from the blood sampling data, with values interpolated smoothly between data points.

Four animals received two injections (the second following five Omniscan half-lives, which is approximately 2.5 hr), yielding nine data sets. For each rat, analysis of tumor and muscle data was performed on the largest (central) tumor slice.

Analysis

RR curves were obtained from 21 contiguous voxels within the perivertebral muscle, while TOIs were obtained from nine to 26 contiguous voxels (depending on tumor size) located within the tumor. Each TOI from each animal and each run was submitted to Eq. [1] with the respective measured AIF for a two-parameter fit (K^{trans} and v_e), and to Eq. [2] with the measured RR for a three-parameter fit ($K^{\text{trans,TOI}}$, $v_{e,\text{TOI}}$, and $K^{\text{trans,RR}}$). In this formulation of the RR model, only a value for $v_{e,\text{RR}}$ need be assumed and we assign a value of 0.08 (see Ref. 16 and references therein). For animals that received two injections, each data set was considered separately with new RRs and TOIs chosen. Considering each injection separately increases the effective number of measurements in the study. While consecutive injections in the same animal could be exploited to study the reproducibility of the technique, the data acquired here were not designed for that type of analysis, and we are in the process of assessing the reproducibility of the RR model (17). Linear regression analysis and a Student's t -test were performed to test for correlation and significant differences between the parameters derived from the two methods. Parameter uncertainties were computed in a manner previously reported (18). Briefly, the average absolute deviation of the data points from the best-fitted curve returned by Eq. [1] is found; that is, we

compute $\delta \equiv \frac{1}{n} \sum_{t_i=t_0}^n |\epsilon(t_i)|$, where $\epsilon t_i \equiv \text{fit}(t_i) - \text{data}(t_i)$.

Then each point in the best-fit curve is summed with a random value from $-\delta$ to $+\delta$, yielding a new “data” set. This new curve is then fit with Eq. [1] to yield a new set of parameters. Repeating this process 100 times yields 100 values for each parameter (i.e., K^{trans} and v_e) from which the means and standard deviations (SDs) are computed. While (perhaps) this approach is not intuitive and lacks validation, this is an accepted method that is appropriate for assessing parameter errors in nonlinear least-squares fitting of the type presented above (19). Indeed, some investigators in this field have called this approach the “only way of making the desired estimation” (19).

A second analysis was conducted in which all AIFs were averaged (after aligning to peak concentration) to produce a “population-based” AIF. The population AIF was obtained by temporally coregistering the peak values of all AIF data vectors and then averaging each time point across all nine measured AIFs. This average AIF was then submitted with each TOI to Eq. [1], and the output parameters were also tested for correlation and significant differences between both the RR values and the values returned from using the individual AIFs.

A third analysis was designed to test the accuracy of the RR model for returning an estimate of $K^{\text{trans,RR}}$, and to test the validity of assigning $v_e = 0.08$. In this analysis the muscle TOI and measured AIF curve from each data were used as input into Eq. [1] to extract K^{trans} and v_e values for the muscle tissue.

Finally, we computed the power of comparing the two methods using the nine paired samples to assess whether the number of studies was sufficient for statistical comparisons. To do this, we first log-transformed the data to ensure that the measurement SD would be independent of

the subject mean (e.g., Ref. 20). We then used the standard analysis to compute the power using a type I error probability of 0.05, $N = 9$, the measured difference in means between the two methods, and the measured within group SD.

RESULTS

Figure 1 illustrates how phase and blood sampling data were combined to calculate the AIF in a representative rat (rat 2, injection 2).

For each TOI, nearly all voxels enhanced significantly after injection of CA. Furthermore, most voxels enhanced to the same degree (i.e., there was very little intratumoral heterogeneity). Figure 2 depicts typical results from this study. Panel a depicts an axial T_2 -weighted cross section of rat 1 (injection 1) with the tumor indicated by the arrow, while panel b depicts the TOI (open circles) with the fit obtained from Eqs. [1] (solid line) and [2] (dashed line), as well as the RR (filled circles). The black circle indicates the TOI, and the white circle indicates the RR. The measured AIF for this rat is shown in the upper right corner. Both Eqs. [1] and [2] describe the data well for this rat tumor. The parameter estimates are similar for the two methods: $K^{\text{trans,TOI}} = 0.11 \pm 0.002 \text{ min}^{-1}$ and $v_{e,\text{TOI}} = 0.34 \pm 0.009$ for Eq. [1], and $K^{\text{trans,TOI}} = 0.13 \pm 0.058 \text{ min}^{-1}$ and $v_{e,\text{TOI}} = 0.45 \pm 0.016$ for Eq. [2]. The results are presented as the mean ± 1 SD. The values of $K^{\text{trans,RR}}$ and $v_{e,\text{RR}}$ obtained by analyzing the RR with Eq. [1] were $0.021 \pm 0.002 \text{ min}^{-1}$ and 0.067 ± 0.01 , respectively, which is in reasonable agreement with the Eq. [2] estimate for $K^{\text{trans,RR}}$ ($0.027 \pm 0.012 \text{ min}^{-1}$) and the assigned value for $v_{e,\text{RR}}$ (0.08). The parameter values are well within the range of K^{trans} and v_e values that have been reported for a variety of tumors (21–24). The mean (absolute) percent difference between the methods was 22.0% (range: -20.8 – 50.3%) for K^{trans} and 28.1% (range: -32.3 – 76.0%) for v_e .

Figure 3 presents a comparison of the $K^{\text{trans,TOI}}$ data obtained by the two methods on a scatter plot with the linear regression plot. The slope of the solid regression line is 0.96 (which is close to the ideal of unity) with an r^2 value of 0.80 ($P = 0.0012$). The dashed lines indicate the 95% confidence intervals. The slopes for the upper and lower lines are 0.80 and 1.11, respectively, which enclose unity. The result of the Student's two-tailed t -test for differences of means is 0.14, which is not statistically significant ($P = 0.88$) and indicates that the two methods yield similar results. Figure 4 presents a similar comparison of the $v_{e,\text{TOI}}$ data obtained by the two methods on a scatter and linear regression plot. The slope of the solid regression line is 0.87 (further from the ideal of unity) with an insignificant r^2 -value of 0.02. The slopes of the dashed 95% confidence intervals are 0.69 and 1.05. It is clear that the v_e values do not vary much between the different tumors, which indicates that the precision of the techniques is not good enough to demonstrate these small differences. The result of the Student's two-tailed t -test for differences of means is 0.85, which is not statistically significant ($P = 0.41$) and indicates that the two methods yield similar results. Of note is that the uncertainty in the Eq. [2] estimates is considerably larger than that in the Eq. [1] output. This point is discussed below.

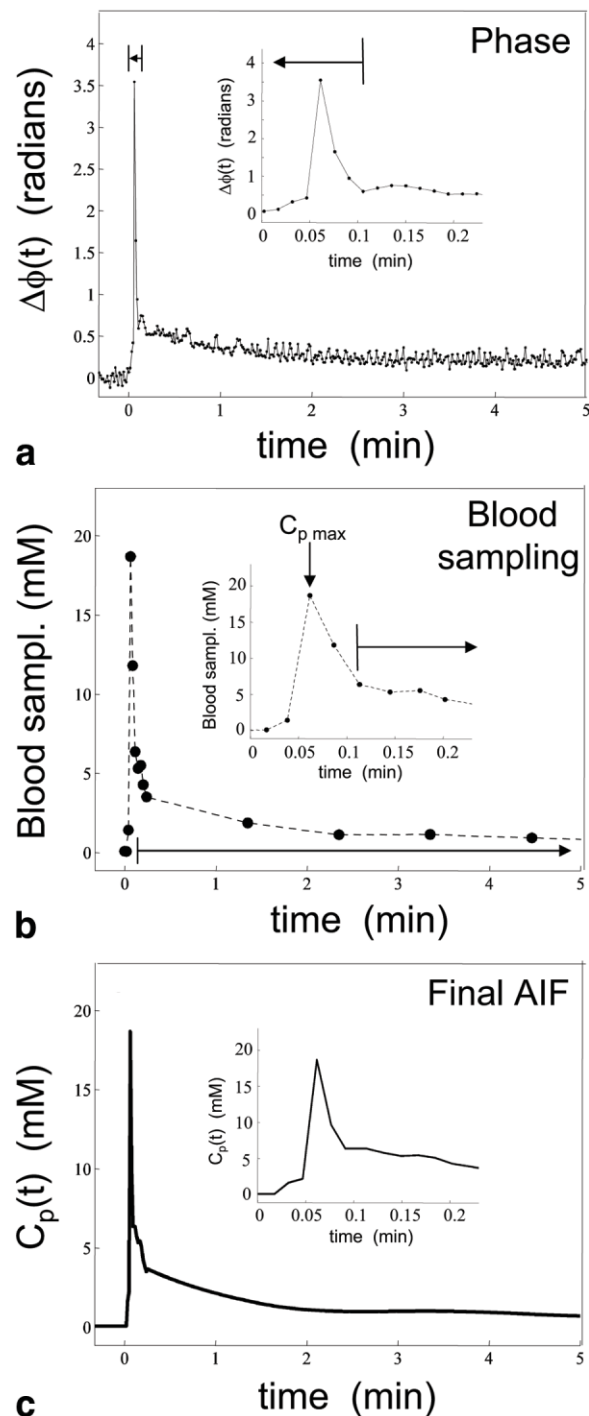
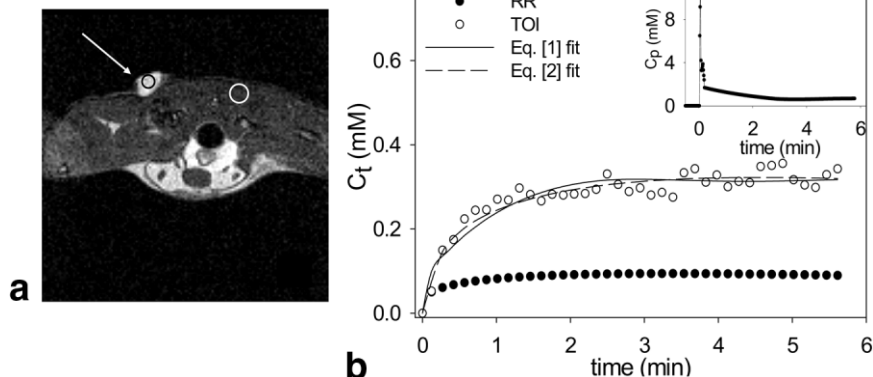


FIG. 1. Illustration of how phase (a) and blood-sampling (b) data were combined to calculate the AIF (c) for a representative rat (rat 2, injection 2). For the fast bolus regime (0.00 to ~ 0.09 min), the AIF was calculated by scaling the phase data to the peak blood-sampling value ($C_{p,\text{max}} = 18.7 \text{ mM}$). For the rest of the AIF ($t > 0.09$ min), the blood-sampling data were used directly (with interpolation) and the phase data were ignored. The time points of the blood sampling data were shifted (if necessary) so that the peak blood sample concentration aligned with the peak of the phase data.

FIG. 2. **a**: T_2 -weighted axial cross section of the tumor indicated by the white arrow. The time course obtained from a 21-voxel ROI within the tumor center is presented as the open circles in panel **b**. The black circle indicates the TOI, and the white circle indicates the RR. The solid and dashed lines indicate the best fit of the data using Eqs. [1] and [2], respectively. The AIF measured from this animal is presented in the upper-right corner of panel **b**.



The second analysis was done to test the notion that a population average AIF could return values similar to those obtained by an individual AIF analysis. The mean (absolute) percent difference between the estimates obtained with the true AIF and the population AIF is 35.8% (range: -71.6 – 19.4%) for $K^{\text{trans,TOI}}$ and 39.0% (range: -65.2 – 5.5%) for $v_{e,\text{TOI}}$. In all but three cases, the group AIF underestimated the $K^{\text{trans,TOI}}$ value returned by the true AIF by $>25\%$, and in all but one case the group AIF underestimated the $v_{e,\text{TOI}}$ value returned by the true AIF by $>25\%$. The Student's t -test returned values of 2.03 and 3.89 and $P = 0.06$ and 0.001 for $K^{\text{trans,TOI}}$ and $v_{e,\text{TOI}}$, respectively. Thus the parameters returned by the population-based AIF are statistically different from those obtained by the true AIF analysis. Moreover, there was no statistically significant correlation (linear regression) between parameters returned by the population AIF analysis and either the true AIF analysis or the RR analysis.

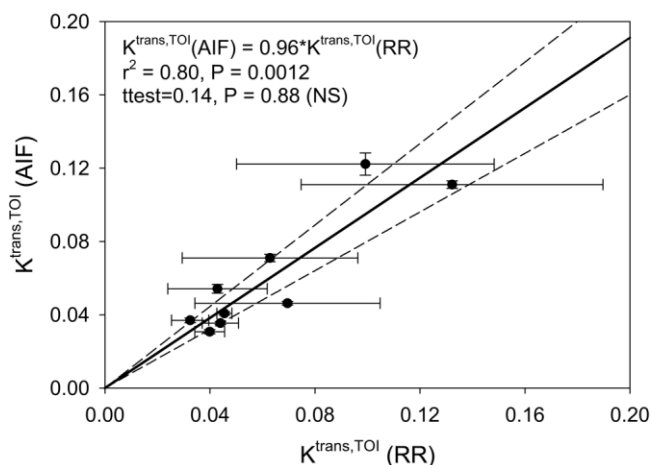


FIG. 3. Scatter plot of $K^{\text{trans,TOI}}$ obtained by the RR model (Eq. [2]) vs. $K^{\text{trans,TOI}}$ obtained by a direct AIF measurement analysis (Eq. [1]). The solid line indicates a best fit of the linear regression line. The slope is 0.96, which is close to the ideal of unity. Of note are the error bars that indicate ± 1 SD of the mean. The RR model presents much lower precision than the standard analysis. This can be markedly improved if a protocol designed more specifically for an RR analysis is employed. See “Results” section in text for details.

The third analysis was conducted to test the accuracy of the Eq. [2] estimates of $K^{\text{trans,RR}}$ and to test the validity of assigning $v_{e,\text{RR}} = 0.08$. The (absolute) percent difference between the methods was 20.3% (range: -22.5 – 31.3%) for $K^{\text{trans,RR}}$, and 27.4% (range: -42.4 – 39.1%) for $v_{e,\text{RR}}$. Of note is that the average $v_{e,\text{RR}}$ value returned by the Eq. [1] analysis of the RR was 0.0797 ± 0.0276 , which agrees with the assigned value of 0.08. This offers additional confidence in assigning $v_{e,\text{RR}} = 0.08$. Figure 5 presents a scatter plot of the $K^{\text{trans,RR}}$ values returned by both methods. The slope is nearly unity (0.98) with an r^2 of 0.76 ($P = 0.0095$). The slopes of the 95% confidence intervals are 0.83 and 1.12, which also enclose unity. The result of the Student's two-tailed t -test is 0.19, which is not significant ($P = 0.85$).

Figures 6 and 7 summarize of the scatter of the estimates of K^{trans} and v_e , respectively, obtained by all analysis methods (direct AIF measurement, RR method, and population-averaged AIF). The data are presented in two ways: the scatter plots indicate individual parameter values with

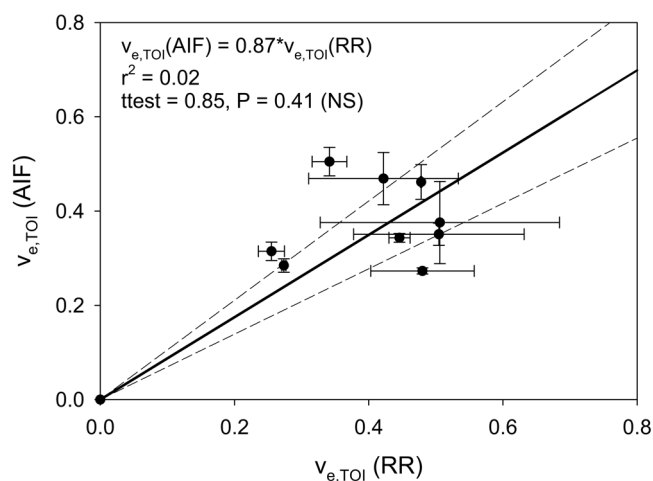


FIG. 4. Scatter plot of $v_{e,\text{TOI}}$ obtained by the RR model (Eq. [2]) vs. $v_{e,\text{TOI}}$ obtained by a direct AIF measurement analysis (Eq. [1]). The solid line indicates a best fit of the linear regression line. The slope is 0.87, even though the r^2 value is extremely low. Note that the v_e values do not vary much between the different tumors, which indicates that the precision of the techniques may not be good enough to demonstrate subtle intratumoral differences.

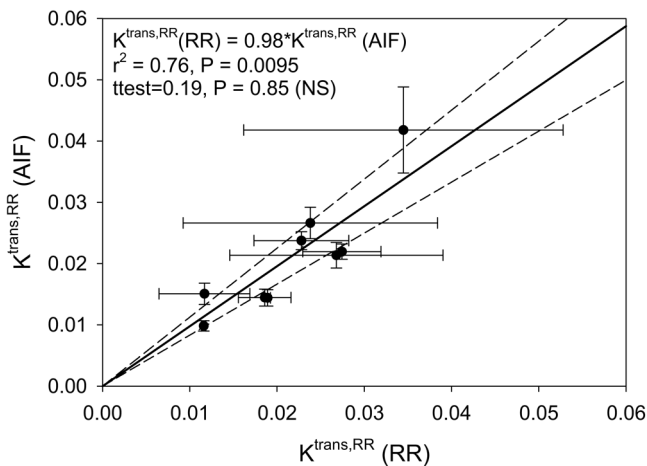


FIG. 5. Scatter plot of $K^{trans,RR}$ obtained by the RR model (Eq. [2]) vs. $K^{trans,RR}$ obtained by a direct AIF measurement analysis (Eq. [1]). The solid line indicates a best fit of the linear regression line. The slope is 0.98, which is nearly unity. This result is of note because it means that $K^{trans,RR}$ can be left as a variable parameter in an RR analysis, and thus one only has to assign a value to $v_{e,RR}$. As presented in the “Results” section of the text $v_{e,RR}$ was returned by the AIF method as 0.0797 ± 0.0276 , which is very nearly identical to the assigned value of 0.08.

error bars (± 1 SD), while the gray bar graphs indicate the mean (bold horizontal line), median (light horizontal line), and the 10th and 90th percentiles. (On several plots each individual percentile is not visible on the scale at which the graphs are presented.) The first two columns of Fig. 6 show the spread of the $K^{trans,RR}$ value as returned by both

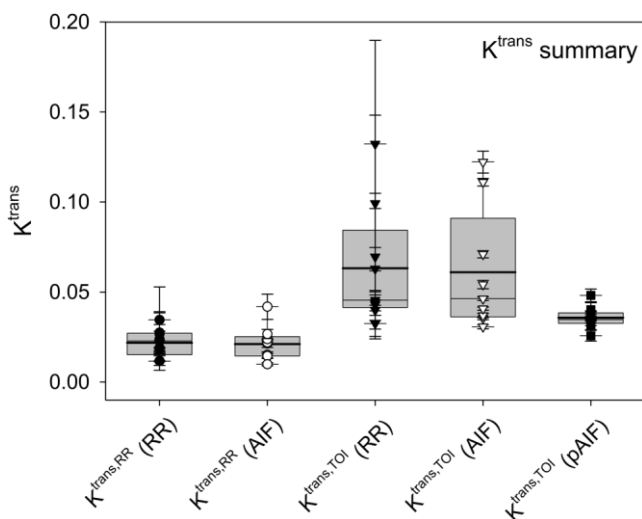


FIG. 6. The $K^{trans,RR}$ and $K^{trans,TOI}$ data are presented as both scatter plots (parameter values ± 1 SD) and bar graphs indicating the mean (bold horizontal line), median (light horizontal line), and 10th and 90th percentiles. While each parameter clusters about common values regardless of the analysis employed, the errors in the $K^{trans,TOI}$ estimated by the RR model (Eq. [2]) are much larger than those reported by the direct AIF measurement method (Eq. [1]). Also note the lack of dynamic range afforded by the population AIF approach (far right).

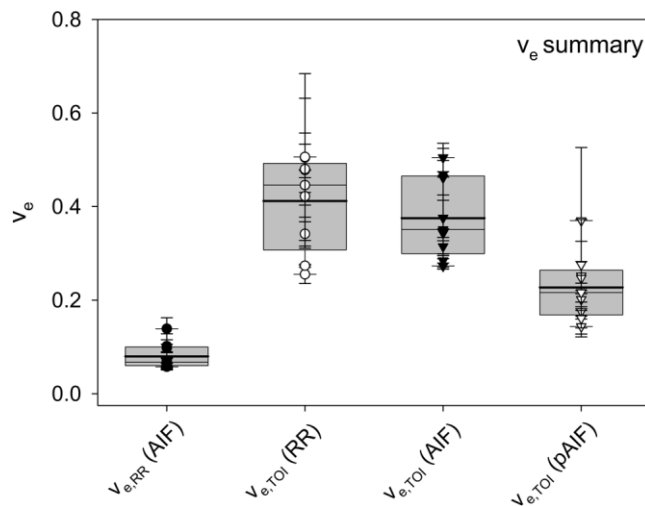


FIG. 7. The analogous plot of Fig. 6 for the v_e parameter. Of particular note is that the values returned for $v_{e,RR}$ by the direct AIF measurement (Eq. [1]) are centered on 0.08, which justifies the value assumed for the three-parameter ($K^{trans,RR}$, $K^{trans,TOI}$, $v_{e,TOI}$) fit of Eq. [2].

the Eq. [1] and [2] analyses. Similarly, columns 3 and 4 display the Eq. [1] and [2] estimates of $K^{trans,TOI}$, in which the uncertainty of the RR method is pronounced. The values returned by the population-based AIF show both small error and small dynamic range, and do not correlate with either the RR or direct AIF measurement approach. Figure 7 displays the analogous plots for v_e , and similar comments apply to these graphs. The value of $v_{e,RR}$ as returned by direct AIF measurement is centered right at 0.08, and this is significant since this is precisely the value chosen to assign $v_{e,RR}$ in the Eq. [2] analysis. This lends support to the assumption of pinning $v_{e,RR}$ at 0.08.

Figure 8 displays all nine AIFs measured in the study, as well as the population-based average AIF. For rats with multiple injections, the two AIFs are displayed on the same axis. Of note is that both the peak concentration and the washout period are greater for the second injection compared to the first injection for each animal. The mean (absolute) difference in peak concentration between the first and second injections was $7.5\% \pm 30.0\%$ (mean ± 1 SD). This could be due to changes in heart and respiratory rates that occurred over the 4-hr experiment, as well as the fact that blood samples were taken from each animal. The mean (absolute) difference between the population average AIF and each injection was $18.3\% \pm 15.6\%$. Thus, in general, there was more variation between the population-based AIF and the individual AIFs than there was between successive AIF measurements of the same animal. The dissimilarity between the population-average AIF and the individual AIFs results in estimated parameter values that are significantly different from those extracted via the RR or direct AIF measurement models, as summarized in Figs. 6 and 7.

In computing the power of the comparisons made here, we follow the approach outlined by Bland and Altman in Ref. 20. We first determine whether the variability in the measurements is independent of the magnitude of the

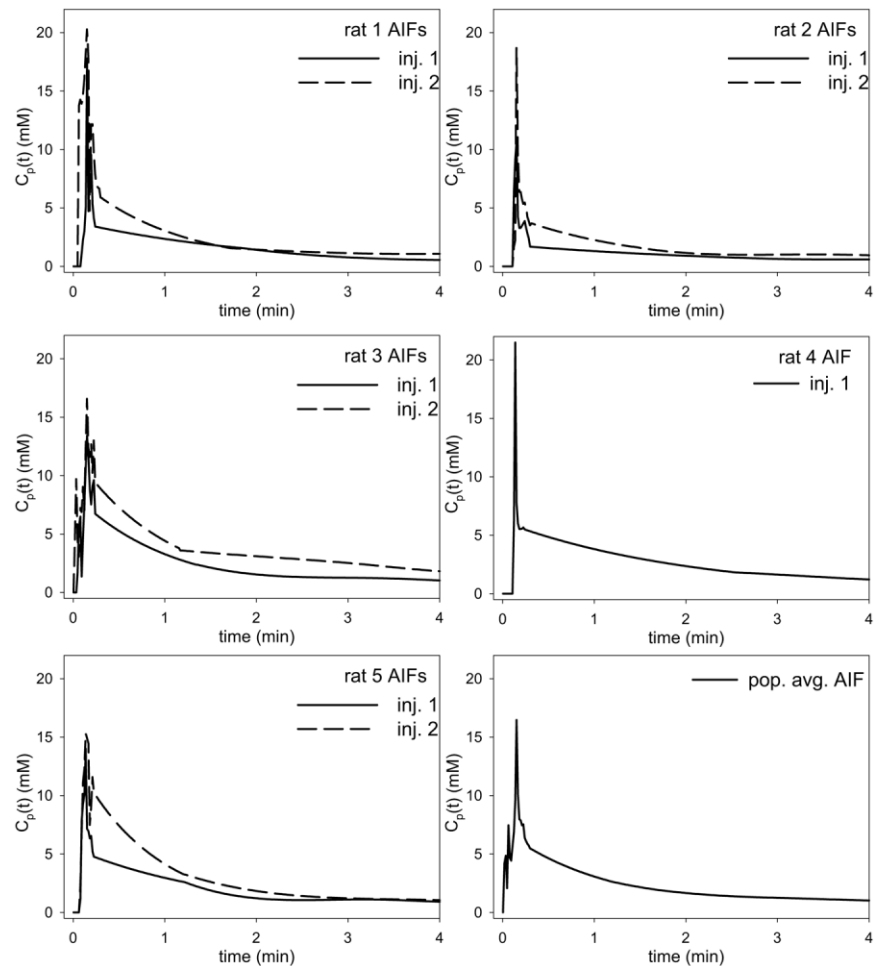


FIG. 8. All nine AIFs measured in the study and the population-based average AIF are shown. If a rat received multiple injections, the two AIFs are displayed on the same axis. The mean difference between the first and second injections was $7.5\% \pm 30\%$, whereas the mean difference between the population-average AIF and each injection was $18.3\% \pm 15.6\%$.

measurement, by testing whether the absolute difference between the two measurements (one measurement for the RR method and one for the AIF method) is proportional to the mean of the two measurements. Kendall's τ -test yielded the following results: $\tau = 0.61$, $P < 0.03$ for $K^{\text{trans,TOI}}$ (Fig. 3); $\tau \approx 0.0$, $P \approx 1.0$ for $v_{e,\text{TOI}}$ (Fig. 4); and $\tau = 0.61$, $P < 0.03$ for $K^{\text{trans,RR}}$ (Fig. 5). Thus, in computing power we use the \log_{10} -transformed data for both K^{trans} comparisons and the raw data for the v_e comparison. For the comparison in Fig. 3, the difference in population (\log_{10}) means (δ) was 0.0899 and the SD of the difference in measurements (σ) was 0.0399, yielding a power of 0.99. For Fig. 4, $\delta = 0.0990$ and $\sigma = 0.0696$, yielding a power of 0.95; and for Fig. 5, $\delta = 0.0839$ and $\sigma = 0.0330$, yielding a power of 0.99. The results of the power analysis indicated that nine samples were sufficient to make statistical comparisons between the two methods on estimates of $K^{\text{trans,TOI}}$, $v_{e,\text{TOI}}$, and $K^{\text{trans,RR}}$.

DISCUSSION AND CONCLUSIONS

In this effort we performed a comparison between the standard approach for DCE-MRI (summarized by Eq. [1]) and an RR method (summarized by Eq. [2]). Equation [1] requires the measurement of an AIF, which requires very high temporal resolution with consequent reductions in

spatial resolution and temporal resolution. Equation [2] alleviates this need by calibrating the enhancement in a TOI (here, a tumor) to that of an RR (here, muscle). The data presented here show that there is a strong and significant correlation between the K^{trans} values extracted by the RR model and those extracted by an AIF-driven analysis. While there was no statistically significant linear relationship between the v_e values output by each model, there was also no statistically significant difference between the values returned, indicating that there may not be much variation inherent in this parameter. Thus, when considering studies of the vascular properties of tumors, parameters reported from a RR model are a reasonable alternative if the AIF cannot be accurately determined. This also means that investigators can design studies with an RR analysis in mind and thus acquire data with a lower temporal resolution, allowing higher spatial resolution and higher SNR. For example, the data for this study were acquired with very high temporal resolution and thus required a voxel size of 1.5 mm^3 to obtain a reasonable SNR of 10. Assuming the exact same $\text{TR}/\text{TE}/\alpha$, FOV, acquisition matrix, and slice thickness as those reported here, but performing the experiment on a 7.0T magnet and using a 38-mm mouse coil would result in an increase in SNR of a factor of ~ 100 . The SNR scales linearly with field strength (25,26), and the filling factor scales as the ratio of the

sample volume being observed to the coil volume (27). Since high temporal resolution is not required for an RR analysis, one could boost the SNR by another factor of 2 simply by acquiring four acquisitions. This additional SNR could be “spent” on obtaining significantly smaller voxels.

The SNR of the data presented in this work was not adequate to perform a voxel-based comparison. The relatively low SNR also revealed a problem inherent in the RR model as presented here, namely, a lack of precision in the parameter estimates. SDs in the parameters output by the RR model frequently approached 50% of the mean value, which is an obvious weakness of employing the RR model in a low-SNR situation. It should be noted that when data are collected with lower temporal resolution to allow for more acquisitions and therefore a higher SNR (exactly the type of data set for which a RR model is designed), the precision increases (9).

We have also shown that a population-based AIF does not compare favorably with individually measured AIFs, which adds further support to earlier findings (28). This suggests one use for the RR model: If the AIF cannot be measured on an individual basis, the data presented here suggest that an RR model is superior to analysis employing a group-averaged AIF. This comment should be tempered, however, by the fact that the effects of maintaining anesthesia for a 4-hr study while extracting significant volumes of blood (for AIF characterization) preclude us from drawing the strong conclusion that a standardized AIF in general is inaccurate.

The results of this study also confirm that the assignment of $v_{e,RR} = 0.08$ for a muscle tissue RR is reasonable. By analyzing the respective RR time courses with the appropriate individual “gold-standard” AIF, we found that the group average value for $v_{e,RR}$ was 0.0797 ± 0.0276 . This reinforces earlier studies (16) and further justifies assigning the parameter this value. Furthermore, simulations indicate that an error of $n\%$ in the assignment of $v_{e,RR}$ leads to an error of $n\%$ in the output of the data. This means that errors from an incorrect $v_{e,RR}$ assignment are considerably less than those arising from application of a population-based AIF. Furthermore, the $K^{trans,RR}$ value returned from the RR analysis was similar to that returned from the AIF-derived method.

An alternative analysis would be to reconstruct the AIF from the muscle curve and compare it with the measured AIF. To do this, one would employ the differential form of the Kety law in conjunction with the muscle parameters $K^{trans,RR}$ (obtained from an Eq. [2] fit) and $v_{e,RR}$ (assigned at 0.08). However, since the data in this study were acquired with high temporal resolution, the SNR was low. Taking a derivative of a noisy function can result in a poorly behaved function. Thus, for our data, this back-calculated AIF resembled the measured AIF only grossly, since the former lacked adequate precision for a proper comparison. However, this may be an interesting avenue to explore with higher-SNR data (e.g., using a higher-performance RF coil, higher field strength, or fewer slices).

Another possible analysis of interest would be to consider the four rats that received two injections and test the reproducibility of the two techniques. Again, the limited spatial resolution and SNR is confounding. Since the two

injections are separated by ~ 2.5 hr, it is very difficult to ensure that one is interrogating the same section of tissue for both injections. Additionally, the arterial blood sampling would lead to a change in blood volume that could result in a reduction of tumor blood flow. Also, the long period of halothane anesthesia (~ 5 hr) may have affected the results. Moreover, over such a long time period, the tumor physiology itself can change. In separate efforts we have investigated the reproducibility of the RR model (17). In these studies, care was taken to obtain high SNR and spatial resolution at the higher field of 7T. Additionally, images were acquired continuously throughout the 5-hr study to allow for proper coregistration. Heart rate and animal temperature were also maintained within $\pm 10\%$ of a mean value.

As a final (limiting) observation, we note that in this study we took the AIF-returned values as the gold standard, and this may have been ill advised. It is known that when the width of the AIF is approximated as a delta function, and the peak of the AIF changes by some percentage, the K^{trans} will change by the same percentage. Though we do not have a delta function for the AIF here, it is quite possible than even higher temporal resolution would be required to ensure that the AIF peak height is measured correctly.

In order for the RR model to gain acceptance, it must be shown to yield results similar to those obtained from more conventional methods, to be reproducible, and to correlate with histology. Here we have shown that the RR model correlates well with the more standard method based on direct measurements of the AIF. A preliminary report assessed the reproducibility of the technique (17). Comparisons with histology are currently under way, and a preliminary report on a technique to make such a correlation has been presented (29). Furthermore, to increase the accuracy of the RR method, the effects of transcytolemmal water exchange should be incorporated into Eq. [2] as they have been in Eq. [1] (18,30). A preliminary report has also been offered on this topic (31).

ACKNOWLEDGMENTS

We thank Erika Peacock and D.M. for technical assistance; Professors James Joers, D. Dean Billheimer, and Baxter P. Rogers for informative discussions; and Lisa Bernas for help with the analysis.

REFERENCES

1. Choyke PL, Dwyer AJ, Knopp MV. Functional tumor imaging with dynamic contrast-enhanced magnetic resonance imaging. *J Magn Reson Imaging* 2003;17:509–520.
2. Tofts PS, Brix G, Buckley DL, Evelhoch JL, Henderson E, Knopp MV, Larsson HBW, Lee T-Y, Mayr NA, Parker GJM, Port RE, Taylor J, Weisskoff RM. Estimating kinetic parameters from dynamic contrast-enhanced T_1 -weighted MRI of a diffusible tracer: standardized quantities and symbols. *J Magn Reson Imaging* 1999;10:223–232.
3. Lankester KJ, Taylor NJ, Stirling JJ, Boxall J, D’Arcy JA, Leach MO, Rustin GJ, Padhani AR. Effects of platinum/taxane based chemotherapy on acute perfusion in human pelvic tumours measured by dynamic MRI. *Br J Cancer* 2005 31;93:979–985.
4. Li KL, Wilmes LJ, Henry RG, Pallavicini MG, Park JW, Hu-Lowe DD, McShane TM, Shalinsky DR, Fu YJ, Brasch RC, Hylton NM. Heterogeneity in the angiogenic response of a BT474 human breast cancer to a novel vascular endothelial growth factor-receptor tyrosine kinase inhibitor: assessment by voxel analysis of dynamic contrast-enhanced MRI. *J Magn Reson Imaging* 2005;22:511–519.

5. Wang B, Gao ZQ, Yan X. Correlative study of angiogenesis and dynamic contrast-enhanced magnetic resonance imaging features of hepatocellular carcinoma. *Acta Radiol* 2005;46:353–358.
6. Kovar DA, Lewis M, Karczmar GS. A new method for imaging perfusion and contrast extraction fraction: input functions derived from reference tissues. *J Magn Reson Imaging* 1998;8:1126–1134.
7. Yang C, Karczmar GS, Medved M, Stadler WM. Estimating the arterial input function using two reference tissues in dynamic contrast-enhanced MRI studies: fundamental concepts and simulations. *Magn Reson Med* 2004;52:1110–1117.
8. Riabkov DY, Di Bella EV. Estimation of kinetic parameters without input functions: analysis of three methods for multichannel blind identification. *IEEE Trans Biomed Eng* 2002;49:1318–1327.
9. Yankeelov, Luci JJ, Lepage M, Li R, Debusk L, Lin C, Price RR, Gore JC. Quantitative pharmacokinetic analysis of DCE-MRI data without an arterial input function: a reference region model. *Magn Reson Imaging* 2005;23:519–529.
10. Lammertsma AA, Bench CJ, Hume SP, Osman S, Gunn K, Brooks DJ, Frackowiak RSJ. Comparison of methods for analysis of clinical [^{14}C]Raclopride studies. *J Cereb Blood Flow Metab* 1999;16:42–52.
11. Harrer JU, Parker GJ, Haroon HA, Buckley DL, Embelton K, Roberts C, Baleriaux D, Jackson A. Comparative study of methods for determining vascular permeability and blood volume in human gliomas. *J Magn Reson Imaging* 2004;20:748–757.
12. Su MY, Wang Z, Roth GM, Lao X, Samoszuk MK, Nalcioğlu O. Pharmacokinetic changes induced by vasomodulators in kidneys, livers, muscles, and implanted tumors in rats as measured by dynamic Gd-DTPA-enhanced MRI. *Magn Reson Med* 1996;36:868–877.
13. Cron GO, Addison C, Wallace JC, Wilkins RC, Fortin T, Pappas BP, Kelcz F, Santyr GE. Does measurement of the arterial input function improve the correlation between tumor microvessel density and MR derived perfusion of small molecular extracellular Gd chelates? In: *Proceedings of the 12th Annual Meeting of ISMRM, Kyoto, Japan, 2004* (Abstract 1965).
14. Cron GO, Santyr G, Kelcz F. Improvement in breast lesion characterization with dynamic contrast-enhanced MRI using pharmacokinetic modeling and bookend T1 measurements. *Magn Reson Med* 2004;51:1066–1070.
15. Cron GO, Wallace JC, Stevens WD, Fortin T, Pappas BA, Wilkins RC, Kelcz F, Santyr GE. A comparison of T2*-weighted magnitude and phase imaging for measuring the arterial input function in the rat aorta following intravenous injection of gadolinium contrast agent. *Magn Reson Imaging* 2005;23:619–627.
16. Donahue KM, Weiskoff RM, Parmelee DJ, Callahan RJ, Wilkinson RA, Mandeville JB, Rosen BR. Dynamic Gd-DTPA enhanced MRI measurement of tissue cell volume fraction. *Magn Reson Med* 1995;34:423–432.
17. Yankeelov TE, Debusk L, Luci JJ, Lin C, Price RR, Gore JC. Reproducibility of the reference region method for the analysis of DCE-MRI data. In: *Proceedings of the 13th Annual Meeting of ISMRM, Miami Beach, FL, USA, 2005* (Abstract 2104).
18. Yankeelov TE, Rooney WD, Xin Li, Springer CS. Variation of the relaxographic “shutter-speed” for transcytolemmal water exchange affects CR bolus-tracking curve shape. *Magn Reson Med* 2003;50:1151–1169.
19. Press WH, Flannery BP, Teukolsky SA, Vetterling WT. *Numerical recipes in C: the art of scientific computing*. Cambridge: Cambridge University Press; 1988. p 548–551.
20. Bland JM, Altman DG. Measurement error proportional to the mean. *Br Med J* 1996;313:106.
21. Graff BA, Benjaminsen IC, Melas EA, Brurberg KG, Rofstad EK. Changes in intratumor heterogeneity in blood perfusion in intradermal human melanoma xenografts during tumor growth assessed by DCE-MRI. *Magn Reson Imaging* 2005;9:961–966.
22. Li KL, Wilmes LJ, Henry RG, Pallavicini MG, Park JW, Hu-Lowe DD, McShane TM, Shalinsky DR, Fu YJ, Brasch RC, Hylton NM. Heterogeneity in the angiogenic response of a BT474 human breast cancer to a novel vascular endothelial growth factor-receptor tyrosine kinase inhibitor: assessment by voxel analysis of dynamic contrast-enhanced MRI. *J Magn Reson Imaging* 2005;22:511–519.
23. McIntyre DJ, Ludwig C, Pasan A, Griffiths JR. A method for interleaved acquisition of a vascular input function for dynamic contrast-enhanced MRI in experimental rat tumours. *NMR Biomed* 2004;17:132–143.
24. Galbraith SM, Maxwell RJ, Lodge MA, Tozer GM, Wilson J, Taylor NJ, Stirling JJ, Sena L, Padhani AR, Rustin GJ. Combretastatin A4 phosphate has tumor antivascular activity in rat and man as demonstrated by dynamic magnetic resonance imaging. *J Clin Oncol* 2003;21:2831–2842.
25. Edelstein WA, Glover GH, Hardy CJ, Redington RW. The intrinsic signal-to-noise ratio in NMR imaging. *Magn Reson Med* 1986;3:604–618.
26. Black RD, Early TA, Roemer PB, Mueller OM, Mogro-Campero A, Turner LG, Johnson GA. A high-temperature superconducting receiver, nuclear magnetic resonance microscopy. *Science* 1993;259:793–795.
27. Hennel JW, Klinowski J. *Fundamentals of nuclear magnetic resonance*. Essex: Longman Scientific and Technical; 1993. p 104–105.
28. Simpson NE, He Z, Evelhoch JL. Deuterium NMR tissue perfusion measurements using the tracer uptake approach: I. optimization of methods. *Magn Reson Med* 1999;42:42–52.
29. Li X, Yankeelov TE, Rosen G, Gore JC, Dawant BM. Multimodal inter-subject registration of mouse brain images. *Proc SPIE Symp Med Imaging* 2006;6144:6144OT.
30. Landis CS, Li X, Telang FW, Coderre JA, Micca PL, Rooney WD, Latour LL, Véték G, Pályka I, Springer CS. Determination of the MRI contrast agent concentration time course in vivo following bolus injection: effect of equilibrium transcytolemmal water exchange. *Magn Reson Med* 2000;44:563–574.
31. Yankeelov TE, Debusk L, Lin C, Gore JC. Incorporating the effects of transcytolemmal water exchange in the reference region model for DCE-MRI analysis. In: *Proceedings of the 14th Annual Meeting of ISMRM, Seattle, WA, USA, 2006* (Abstract 390).